
B1 (2): Optimization of reactive flows in a single channel of a catalytic monolith: conversion of ethane to ethylene

H. G. Bock¹, O. Deutschmann², S. Körkel¹, L. Maier², H. D. Minh¹, J. P. Schlöder¹, S. Tischer², and J. Warnatz¹

¹ Interdisciplinary Center for Scientific Computing, University of Heidelberg

² Institute for Chemical Technology and Polymer Chemistry, University of Karlsruhe

1 Introduction

The application of so-called short-contact-time reactors to the autothermal production of ethylene from ethane has led to a promising technology. In these devices, mixtures of ethane, oxygen, and nitrogen (and possibly hydrogen) flow through a ceramic monolith coated with a catalytic metal such as platinum. Mild heating of the reactor initiates an autocatalytic reaction that yields a mixture of ethylene, carbon monoxide, hydrogen, water, and smaller amounts of other hydrocarbons. The residence time in the reactor is typically a few milliseconds and the reactor temperatures appear to be in the range 900 – 1000 °C. Experiments with platinum-catalyzed systems show that ethane conversions and ethylene selectivity comparable to conventional steam cracking can be achieved [ZAWD00].

One of the questions arising is the role that homogeneous reactions play in the oxidative dehydrogenation at high temperatures and short contact times. While Huff and Schmidt [HS93] proposed a purely heterogeneous mechanism, experiments by Beretta et al. provided evidence for a major influence of gas-phase reactions [BRF01]. The catalyst may serve as a heat supply by supporting complete combustion of hydrocarbons, and thus initiating endothermic gas-phase reactions.

In a first step, a single channel of a monolithic reactor is modeled. We assume that the cross-section of the channel can be approximated by a cylindrical shape. The inlet conditions and the wall temperature profile are given parameters, which in a second step become subject to the optimization. Detailed models for transport processes as well as for gas-phase and surface reactions are applied to the numerical simulation.

2 Simulation

2.1 General Mathematical Formulation

Modeling of the fluid dynamical process: boundary layer equations

To model flows in a channel, we employ the boundary layer equations which are a simplification of the Navier-Stokes equations. Since our considered channel is an axisymmetrical cylinder, we assume that the flow in it is also axisymmetrical, which can be described by two spatial coordinates, namely the axial one z and the radial one r . By applying von Mises transformation

$$\psi = \int_0^r \rho u r' dr',$$

where ψ is the stream variable, u is the axial velocity and ρ is the mass density, we obtain the following equation system, which we use for modeling the reactive flow in channel of monoliths. Here, we assume that the system is in a steady state. Figure 1 shows a typical catalytic monolith with flow conditions and the model assumption.

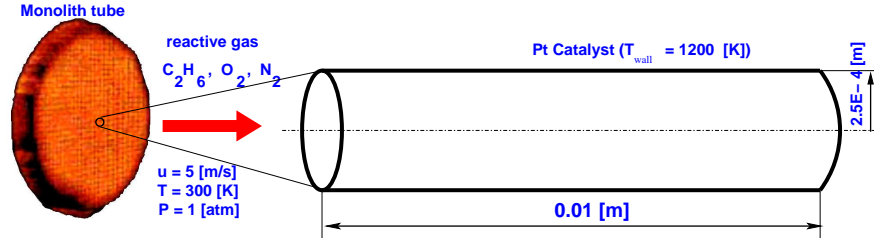


Fig. 1. Catalytic Monolith

Momentum equation:

$$\rho u \frac{\partial u}{\partial z} + \frac{\partial p}{\partial z} = \rho u \frac{\partial}{\partial \psi} \left(\rho u \mu r^2 \frac{\partial u}{\partial \psi} \right), \quad (1)$$

$$\frac{\partial p}{\partial \psi} = 0. \quad (2)$$

Energy equation:

$$\rho u c_p \frac{\partial T}{\partial z} = \rho u \frac{\partial}{\partial \psi} \left(\rho u \lambda r^2 \frac{\partial T}{\partial \psi} \right) - \sum_{k=1}^{N_g} \dot{\omega}_k W_k h_k - \rho u r \sum_{k=1}^{N_g} J_{kr} c_{pk} \frac{\partial T}{\partial \psi}. \quad (3)$$

Species equation:

$$\rho u \frac{\partial Y_k}{\partial z} = \dot{\omega}_k W_k - \rho u \frac{\partial}{\partial \psi} (r J_{kr}), \quad (k = 1, \dots, N_g). \quad (4)$$

State equation:

$$\rho = \frac{P\bar{W}}{RT}. \quad (5)$$

This equation is used for calculating ρ . The relation between the stream variable ψ and the radial variable r is

$$\frac{\partial r^2}{\partial \psi} - \frac{2}{\rho u} = 0. \quad (6)$$

The meaning of the notations used above and in the following is as follows.

- z and r are the cylindrical coordinates.
- u and v are the axial and radial components of the velocity vector.
- p is the pressure.
- T is the temperature.
- Y_k is the mass fraction of the k th species.
- μ is the viscosity.
- ρ is the mass density.
- c_p is the heat capacity of the mixture.
- λ is the thermal conductivity of the mixture.
- c_{pk} is the specific heat capacity of the k th species.
- J_{kr} is the radial component of mass flux vector of the k th species.
- $\dot{\omega}_k$ is the rate of production of the k th species by gas phase reactions.
- h_k is the specific heat enthalpy of the k th species.
- W_k is the molecular weight of the k th species.
- N_g is the total number of gas phase species.
- K_g is the total number of elementary reactions.
- \bar{W} is the mixture mean molecular weight.
- R is the universal gas constant.

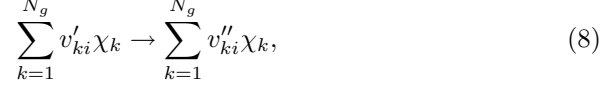
Note that $\mu = \mu(Y, T)$, $\lambda = \lambda(Y, T)$, $c_p = c_p(Y, T)$, $c_{pk} = c_{pk}(Y, T)$, $h_k = h_k(Y, T)$, $\dot{\omega}_k = \dot{\omega}_k(Y, T, p)$, $Y = (Y_1, Y_2, \dots, Y_{N_g})$, and the diffusion flux J_{kr} is given by

$$J_{kr} = -D_k^m \frac{W_k}{\bar{W}} \rho \frac{\partial X_k}{\partial r} - \frac{D_k^T}{T} \frac{\partial T}{\partial r}, \quad (7)$$

where D_k^m and D_k^T are diffusion coefficients, X_k is the mole fraction of the k th species. More details can be found in, e.g., [CKM84], [KCG03] and [RKD⁺00].

Modeling of the chemical process in the gas phase

When moving in a channel, the gas mixture takes part in several chemical reactions. To model this process, we use the detailed chemistry describing elementary reactions on molecular level, the description and derivation of which can be found, e.g., in [WDM96, Deu00]. A chemical reaction involving N_g species can be represented in the general form



where v'_k and v''_k are the stoichiometric coefficients of the k th species and χ_k is the chemical symbol for the k th species and i denotes the reaction number. The rate of production $\dot{\omega}_k$ of the k th species, which appears in equations (4) and (3), is determined by

$$\dot{\omega}_k = \sum_{i=1}^{K_g} v_{ki} k_{fi} \prod_{j=1}^{N_g} [X_j]^{v'_{ji}} \quad (k = 1, \dots, N_g), \quad (9)$$

where

$$v_{ki} := v''_{ki} - v'_{ki},$$

$[X_j]$: the concentration of the j th species,

k_{fi} : the forward rate coefficient of the i th reaction.

The forward rate coefficient k_{fi} is calculated by the Arrhenius expression:

$$k_{fi} = A_i T^{\beta_i} \exp\left(-\frac{E_{ai}}{RT}\right) \quad (i = 1, \dots, K_g), \quad (10)$$

where

A_i : the pre-exponential factor of the i th reaction
[the units are given in terms of m, mol, and s],

β_i : the temperature exponent of the i th reaction,

E_{ai} : the activation energy of the i th reaction [J/mol],

R : the universal gas constant being 8.314 [J/(mol · K)],

T : the gas temperature [K].

The backward (reverse) rate coefficient k_r is determined based on the chemical equilibrium.

The mass fractions Y_k of the species are computed from the concentrations

$$Y_k = \frac{W_k [X_k]}{\sum_{j=1}^{N_g} W_j [X_j]}. \quad (11)$$

They must satisfy

$$0 \leq Y_k \leq 1 \quad (k = 1, \dots, N_g), \quad \sum_{k=1}^{N_g} Y_k = 1. \quad (12)$$

Modeling of the surface chemistry

The chemistry source term \dot{s}_i appearing later in the boundary conditions (17) and (19) states the creation or depletion rate of the i th species due to the adsorption/desorption process and is given by

$$\dot{s}_i = \sum_{k=1}^{K_s} \nu_{ik} k_{fk} \prod_{j=1}^{N_g+N_s} [X_j]^{v'_{jk}}, \quad (13)$$

where K_s and N_s are the numbers of elementary surface reactions and of adsorbed species, respectively. If the j th species is a gas-phase species then $[X_j]$ is its concentration, otherwise, if it is a surface species then $[X_j] = \theta_i \Gamma$, where θ_i is the surface coverage and Γ the surface site density.

Depending on the reaction mechanism, in some reactions, the rate coefficient k_{fk} is calculated by the standard Arrhenius formula

$$k_{fk} = A_k T^{\beta_k} \exp\left(-\frac{E_{ak}}{RT}\right), \quad (14)$$

and in some other reactions, it is described by the modified Arrhenius formula

$$k_{fk} = A_k T^{\beta_k} \exp\left(-\frac{E_{ak}}{RT}\right) \prod_{i=1}^{N_s} \theta_i^{\mu_{ik}} \exp\left(\frac{\epsilon_{ik} \theta_i}{RT}\right) \quad (15)$$

where μ_{ik} and ϵ_{ik} are surface parameters, and θ_i is surface coverage, which must satisfy

$$0 \leq \theta_i \leq 1 \quad (i = 1, \dots, N_s), \quad \sum_{i=1}^{N_s} \theta_i = 1. \quad (16)$$

2.2 Initial and boundary conditions

As initial conditions, the values of u , p , T , and Y_k are specified at the inlet of the channel:

$$u = u_0, \quad p = p_0, \quad T = T_0, \quad Y_k = Y_{k0} \quad (k = 1, \dots, N_g) \quad \text{at } z = 0.$$

At $\psi = 0$, which corresponds to the centerline of the cylindrical channel, we can deduce the following boundary conditions from the assumed axisymmetry

$$r = 0, \quad \partial u / \partial \psi = 0, \quad \partial p / \partial \psi = 0, \quad \partial T / \partial \psi = 0, \quad \partial Y_k / \partial \psi = 0.$$

At $\psi = \psi_{\max}$ which is defined as

$$\psi_{\max} = \int_0^{r_{\max}} \rho u r' dr' \Big|_{z=0},$$

and corresponds to the channel wall, it holds

$$r = r_{\max}, \quad u = 0, \quad T = T_{\text{wall}}.$$

In addition, since an essential part of chemical reactions takes place at the catalytic wall and because of the state steady assumption, the gas species mass flux produced by heterogeneous chemical reactions and the mass flux of that species in the gas must be balanced there, i.e.

$$\dot{s}_k W_k = -J_{kr} \quad (k = 1, \dots, N_g), \quad (17)$$

where \dot{s}_k is the rate of creation/depletion of the k th gas-phase species by surface reactions. Note that J_{kr} represent the radial components of the diffusive flux vector pointing from the center to the wall. In general we additionally have to take the convective flux $\rho Y_k v_{\text{Stef}}$ into account, where v_{Stef} is the Stefan velocity calculated by

$$v_{\text{Stef}} = \frac{1}{\rho} \sum_{k=1}^{N_g} \dot{s}_k W_k.$$

At the steady state, the Stefan velocity vanishes. Also due to the steady state assumption, the surface coverage θ_i does not depend on time, i.e. $\partial\theta_i/\partial t = 0$. By definition,

$$\frac{\partial\theta_i}{\partial t} = \frac{\dot{s}_i}{\Gamma} \quad (i = N_g + 1, \dots, N_g + N_s). \quad (18)$$

Hence, we have

$$\dot{s}_i = 0 \quad (i = N_g + 1, \dots, N_g + N_s). \quad (19)$$

Equations (17)–(19) stand for the reactions at the catalytic surface, which play a crucial role in the whole physical-chemical process.

The solution of the boundary equation is crucial since it strongly influences the solution of the whole PDE system. Later in this paper we discuss how we compute consistent boundary values.

By (7), (13), (15), and (17), these equations are highly nonlinear with respect to the unknowns Y_k and θ_i . This fact causes major difficulties in the numerical treatment and makes an essential difference between our problem and the one without catalytic surface.

Note that the boundary conditions of our PDEs are not standard ones, such as *Dirichlet conditions* where the dependent variables are explicitly specified at the boundary or *Neumann conditions* where the first-order derivatives of dependent variables are known, but they are given as the algebraic equations (17) and (19).

Using subscript for denoting partial derivatives and the abbreviations

$$\mathcal{E} = \begin{bmatrix} \rho u u_z + p_z \\ 0 \\ \rho u c_p T_z \\ 0 \\ \rho u Y_{1z} \\ \vdots \\ \rho u Y_{N_g z} \end{bmatrix}, \quad \mathcal{F} = \begin{bmatrix} \rho u (\rho \mu r^2 u_\psi)_\psi \\ p_\psi \\ \rho u (\rho u \lambda r^2 T_\psi)_\psi - \sum_{k=1}^{N_g} \dot{\omega}_k W_k h_k - \rho u r \sum_{k=1}^{N_g} J_{kr} c_{pk} T_\psi \\ \frac{\partial r^2}{\partial \psi} - \frac{2}{\rho u} \\ \dot{\omega}_1 W_1 - \rho u (r J_{1,r})_\psi \\ \vdots \\ \dot{\omega}_{N_g} W_{N_g} - \rho u (r J_{N_g,r})_\psi \end{bmatrix}$$

equations (1), (2), (3), (4), and (6) can be summarized to the system

$$\mathcal{E} = \mathcal{F}, \quad (20)$$

which forms, along with (5) and (17)–(19), our entire mathematical model. Next, we discuss how to solve this problem numerically.

2.3 Simulation Method

Semi-discretization

We choose the approach of semi-discretization of the PDE system in the direction ψ by the *method of lines* [Sch91]. Here, we have two independent spatial variables z and ψ , but do not have the independent variable “time”. The axial direction z is now treated as the time-like direction.

The considered interval of ψ is discretized by ψ_i , $i = 1, \dots, N$. Let us denote the function section corresponding to $\psi = \psi_i$ by the subscript i . For instance,

$$u_i := u_i(z) := u(z, \psi_i).$$

This rule is also applied to partial derivatives, e.g.,

$$u_{\psi_i} := u_{\psi_i}(z) := \left. \frac{\partial u(z, \psi)}{\partial \psi} \right|_{\psi=\psi_i}$$

and other quantities, such as temperature T , pressure p , radial coordinate r , and mass fraction Y_k .

Let $\mathcal{A} = (A_{j,k})$ be the matrix defined by

$$A_{j,k} = \begin{cases} \rho u, & \text{if } j = k = 1 \text{ and } 5 \leq j = k \leq N_g + 4 \\ 1, & \text{if } j = 1, k = 2 \\ \rho u c_p, & \text{if } j = k = 3 \\ 0, & \text{otherwise.} \end{cases}$$

and let

$$\mathcal{Q} = [u, p, T, r, Y_1, Y_2, \dots, Y_{N_g}].$$

Then we have

$$\mathcal{E} = \mathcal{A} \mathcal{Q}_z^T. \quad (21)$$

By our convention,

$$\mathcal{E}_i = \mathcal{E}|_{\psi=\psi_i}, \mathcal{A}_i = \mathcal{A}|_{\psi=\psi_i}, \mathcal{Q}_i = \mathcal{Q}|_{\psi=\psi_i}, \mathcal{Q}_{zi} = \mathcal{Q}_z|_{\psi=\psi_i}.$$

With

$$\begin{aligned} E &= [\mathcal{E}_1^T, \mathcal{E}_2^T, \dots, \mathcal{E}_{N-1}^T]^T, \\ A &= \text{diag}(\mathcal{A}_i), \\ Q &= [\mathcal{Q}_1, \mathcal{Q}_2, \dots, \mathcal{Q}_{N-1}], \\ Q_z &= [\mathcal{Q}_{z1}, \mathcal{Q}_{z2}, \dots, \mathcal{Q}_{zN-1}], \end{aligned}$$

(21) implies

$$E = A Q^T,$$

which is the discretization result of the left-hand side of equation (20).

\mathcal{A}_i depends on ρ_i, u_i , and c_{p_i} , which in turn depend only on \mathcal{Q}_i . Note that $\mathcal{A}_i, i = 1, \dots, N-1$, are band matrices with upper bandwidth equal to 1 and lower bandwidth equal to 0. Therefore, A inherits this property, too.

We use the forward finite difference to approximate p_ψ :

$$p_{\psi_i} = \frac{p_{i+1} - p_i}{\psi_{i+1} - \psi_i}. \quad (22)$$

Central finite differences are applied to the following partial derivatives with respect to ψ :

$$u_\psi, T_\psi, (\rho u \mu r^2 u_\psi)_\psi, (\rho u \lambda r^2 T_\psi)_\psi, (r J_{kr})_\psi, \text{ and } X_{k\psi}. \quad (23)$$

(Note that $X_{k\psi}$ does appear in J_{kr} as given in (7).)

The fourth component of \mathcal{F} is discretized by the trapezoidal rule:

$$\left[\frac{\partial r^2}{\partial \psi} - \frac{2}{\rho u} \right]_i = \frac{r_i^2 - r_{i-1}^2}{\psi_i - \psi_{i-1}} - \frac{4}{\rho_i u_i + \rho_{i-1} u_{i-1}}. \quad (24)$$

In addition, we have the boundary condition $r_1 = 0$.

Let F_i denote the semi-discretized form of $\mathcal{F}_i = \mathcal{F}|_{\psi=\psi_i}$ by using the approximation scheme described in (22), (23), and (24). Then

$$F = [F_1^T, F_2^T, \dots, F_{N-1}^T]^T$$

is the discretization result of the right-hand side of equation (20). Note that $F = F(Q)$. Due to the central finite difference scheme, F_i depends on the values at three points ψ_{i-1}, ψ_i , and ψ_{i+1} , i.e., $F_i = F_i(Q_{i-1}, Q_i, Q_{i+1})$.

Hence, the PDE system (20) corresponds to

$$A(Q)Q_z^T = F(Q). \quad (25)$$

With

$$P = \begin{cases} \dot{s}_k W_k + J_{kr}|_{\psi=\psi_N}, & \text{if } 1 \leq k \leq N_g \\ \dot{s}_k, & \text{if } N_g + 1 \leq k \leq N_g + N_s \end{cases}$$

the boundary conditions (17)–(19) can be written as

$$0 = P. \quad (26)$$

Initial conditions are

$$u = u_0, p = p_0, T = T_0, Y_k = Y_{k0} \quad (k = 1, \dots, N_g) \text{ at } z = 0. \quad (27)$$

At the channel wall, u , T , p , and r must fulfill

$$0 = \begin{bmatrix} u \\ p \\ T \\ r \end{bmatrix}_{\psi=\psi_N} - \begin{bmatrix} 0 \\ p_{N-1} \\ T_{\text{wall}} \\ r_{\text{max}} \end{bmatrix}. \quad (28)$$

Finally, the equations (25)–(28) together form the Differential Algebraic Equation (DAE) system with the unknowns

$$[Q_1, Q_2, \dots, Q_N, \theta_1, \dots, \theta_{N_s}],$$

which satisfy, in addition, conditions (12) and (16).

Note that $\theta_1, \dots, \theta_{N_s}$ appear in the formulas to compute \dot{s}_k .

It is worth to say that the partial derivatives of the left- and right-hand side of the DAE with respect to the unknowns and the iteration matrix are of band structure, with total bandwidth $3 \times \dim(Q_i)$. The mentioned band structure arises from choosing suitable indices for Q and F . It is used for efficient computation and storage of derivatives and iteration matrix.

Solution of the DAE system

Since the DAE system is derived from the discretization of a PDE and it contains the model of chemical reaction kinetics, it is stiff. The DAE is of index 1. Therefore we choose an implicit integration method, based on Backward Differentiation Formulas (BDF) for the solution of the initial value problems. For the practical computation, based on the code DAESOL [BBS99, BFD⁺97], we develop a new code that allows us to solve this problem. Features of this code are variable step size and variable order controlled by error estimation, modified Newton's method for the solution of the implicit nonlinear problems, a monitor strategy to control the computation and decomposition of the Jacobian and Internal Numerical Differentiation for the computation of derivatives of the solution w.r.t. initial values and parameters.

In our problems the linear systems arising in Newton's method are very ill-conditioned. We have developed an appropriate scaling. The variables are scaled with the same weighting vector that is used in the BDF error estimation and then we perform row equilibration. The scaling factors are chosen to be integer powers of the machine base in order to avoid scaling roundoff errors. Using this technique the condition number of the linear system is reduced from more than 10^{18} to around 10^7 .

The BDF method needs derivatives of the DAE model functions. Here, we exploit the band structure. Instead of computation of the full Jacobian, we apply a compression technique which only requires few directional derivatives. We use Automatic Differentiation (implemented in the tool ADIFOR [BCH⁺95]) which allows us to compute derivatives with accuracy up to machine precision. This is crucial for a fast performance of the overall solution method.

To solve the DAE, we supply consistent initial values for the algebraic variables. During the integration the consistency is preserved because the algebraic constraints and the equation from the implicit integration scheme are solved simultaneously.

Computation of consistent initial values of the DAE

To integrate the DAE system (25)–(28), a set of consistent initial values is needed. Some of them are explicitly given, as stated in section 2.2. But the mass fractions Y_k ($k = 1, \dots, N_g$) at the catalytic wall $\psi = \psi_N$ and the surface coverage fractions θ_i ($i = 1, \dots, N_s$) are only implicitly determined by the nonlinear equations at the boundary (26) and the constraints (12) and (16).

These equations are highly nonlinear due to the Arrhenius kinetics. The solution is the steady state of a dynamic system of the surface process. The steady state is an asymptotic limit of the corresponding transient system. We only know initial values of the transient system, which can change very drastically until the system goes to steady state. It is very difficult to find values that are sufficiently close to the consistent values in order to have convergence of a Newton type method. Techniques of globalization of the convergence often fail because non-singularity of the Jacobian cannot be guaranteed. Therefore, we use a time-stepping method for solving the corresponding transient system to find an initial guess close to the solution and then apply Newton's method to converge to the solution.

With the variables $(Y_{1N}, \dots, Y_{N_g N}, \theta_1, \dots, \theta_{N_s}) \in \mathbb{R}^{N_g + N_s}$ the nonlinear equation system for the boundary is

$$\dot{s}_k W_k + J_{kr}|_{\psi=\psi_N} = 0 \quad (k = 1, \dots, N_g) \quad (29)$$

$$\dot{s}_k = 0 \quad (k = N_g + 1, \dots, N_g + N_s). \quad (30)$$

The left-hand sides of equation (30) \dot{s}_k , ($k = N_g + 1, \dots, N_g + N_s$) are the rates of creation/depletion of the surface coverage of the surface species multiplied

by the site density Γ :

$$\frac{\partial \theta_i}{\partial t} = \frac{\dot{s}_k}{\Gamma} \quad (k = N_g + 1, \dots, N_g + N_s). \quad (31)$$

Similarly, the left-hand side of equation (29) can be considered as the mass rate of creation/depletion of the k th gas species by surface reactions and diffusion process multiplied by a some length dr , i.e.,

$$\rho dr \frac{\partial Y_k}{\partial t} = \dot{s}_k W_k + J_{kr}|_{\psi=\psi_N} \quad (k = 1, \dots, N_g). \quad (32)$$

The differential equations (31) and (32) describe the corresponding transient state model for the nonlinear equations (29) and (30).

Starting from initial values for mass fractions and surface coverage at the beginning $(Y_{1N}, \dots, Y_{N_g N}, \theta_1, \dots, \theta_{N_s})(t_0)$ we integrate the ODE (31)–(32) until it nearly reaches steady state. In our implementation, we monitor the value of $\|P\|$, when it decreases below a certain value then we switch to Newton’s method. From our practical experience, this method is quite stable even for ill-conditioned problems.

The system (31)–(32) describes a chemical process modeled using detailed chemistry and therefore is very stiff. For solution, we also use the BDF method implemented in the new DAESOL.

To speed up the computation, we only integrate until we are near steady state and then use Newton’s method for fast convergence. Therefore, we do not need high tolerance for the ODE integration which makes the integration procedure fast.

It is interesting to note that the conditions (12) and (16) are satisfied during the integration of ODE if they are fulfilled at the initial and the corresponding ODE model has a physical meaning.

2.4 Simulation Results

The presented methods have been implemented in the software package BLAYER. The software has been developed for general reaction schemes and can be applied for any arbitrary process in a catalytic monolith with detailed gas-phase and surface chemistry.

The user of the software has to provide the reaction mechanism and thermodynamic data, the initial and boundary values, i.e., velocity, gas temperature, pressure and mass or mole fractions of the gas species at the inlet and the surface temperature at the wall. Output of the software are the trajectories of the state variables in Tecplot format.

In the following we present simulation results for the process of conversion of ethane to ethylene. The chemical reactions are modeled by detailed elementary-step reaction mechanisms featuring 261 gas-phase [Kar97] and 82 surface reactions [ZAWD00] involving 25 gas-phase and 20 surface species. This leads to 29 PDEs.

The channel has the length $z_{\max} = 0.01$ [m] and the radius $r_{\max} = 2.5 \times 10^{-4}$ [m].

At inlet the mass fractions are $X_{\text{C}_2\text{H}_6} = 0.44$, $X_{\text{O}_2} = 0.26$ and $X_{\text{N}_2} = 0.30$. All other gases do not occur at the inlet. The inlet gas temperature is $T_{\text{gas}} = 650$ [K] and surface temperature is $T_{\text{wall}} = 930$ [K]. The inlet velocity has the value $u_0 = 0.5$ [m/s].

For the simulation, we use a spatial grid with 20 grid points. Figure 2 shows the trajectories of selected species.

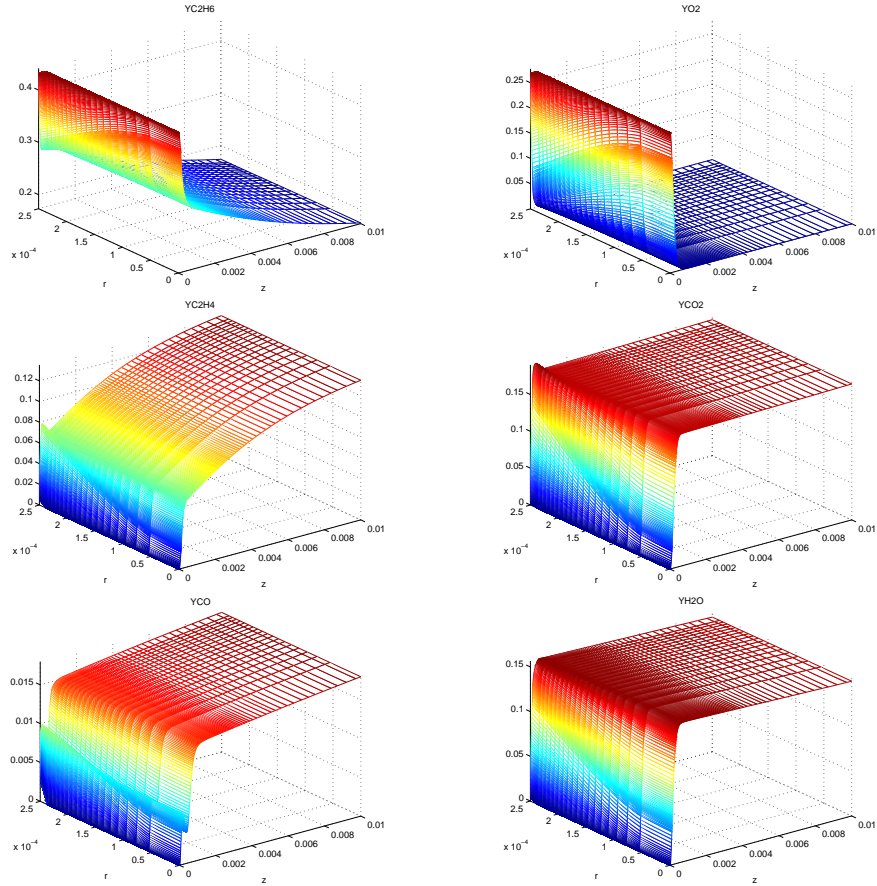


Fig. 2. Simulation results for the conversion of ethane to ethylene, trajectories of ethane, oxygen, ethylene, carbon dioxide, carbon monoxide and water.

The computational time for one simulation run is 30 seconds on a 2.5 GHz Pentium 4 Linux PC.

2.5 Chemical Interpretation of the Results

Figure 2 illustrates typical trajectories for the species concentrations during the oxidative dehydrogenation of ethane to ethylene. The oxygen is consumed completely within the first millimeter of the reactor. Ethane is combusted completely, giving mainly CO_2 and water. The gradients in the concentration profiles for these species indicate that catalytic surface reactions dominate the oxidation.

The dehydrogenation of ethane is a much slower process. The gradients in the species concentrations vanish. Therefore the process is kinetically controlled. This can be achieved by either gas-phase reactions or by slow surface reactions. The continuous formation of CO is due to the water-gas-shift reaction.

3 Optimization

3.1 Formulation of an Optimal Control Problem

In the catalytic combustion process, the initial and boundary conditions can be used to optimize the performance of the reactor, e.g., maximize the gas conversion or maximize the selectivity. In particular, at the inlet of the catalytic monolith, the mass or molar fractions of the species, or the initial velocity $u(r, z)|_{z=0}$, or the initial temperature $T(r, z)|_{z=0}$ can be changed resp. be optimized, and at the catalytic wall, the temperature profile $T_{\text{wall}}(z)$ can be controlled. Moreover, the length of the catalytic tube z_{max} can be optimized.

In a general formulation, this optimization problem can be stated as

$$\min_{w, q} \phi(w) \quad (33)$$

$$\text{subject to} \quad \text{PDE Model Equations}(w, q) \quad (34)$$

$$\text{Initial and Boundary Conditions}(w, q) \quad (35)$$

$$\text{State and Control Constraints}(w, q) \quad (36)$$

where the PDE equations describe the fluid dynamical process (1)-(5) and the gas-phase (9)-(10) chemistry. The initial and boundary conditions are described in (17)-(19) and contain in particular the surface chemistry (13)-(16). w denotes the state vector $w = (u, p, T, r, Y_1, Y_2, \dots, Y_{N_g}, \theta_1, \dots, \theta_{N_s})$ and q are the controls.

For practical reasons, there are often equality and inequality constraints on the control and state variables, such as an upper and lower bounds for the wall temperature, or sum of all mass fractions must be one.

Again, as described above, we semi-discretize the PDE using the method of lines on the grid ψ_i , $i = 1, \dots, N$. This transforms the optimal control problem in a PDE (33)-(36) to an optimal control problem in a DAE which, using the notation of section 2.3, can be written as

$$\min_{x,q} \Phi(x, q) \quad (37)$$

$$\text{subject to } A(Q)Q_z^T = F(Q) \quad (38)$$

$$0 = s_k W_k - J_{kr} |_{\psi=\psi_N}, \text{ if } 1 \leq k \leq N_g \quad (39)$$

$$0 = \dot{s}_k, \text{ if } N_g + 1 \leq k \leq N_g + N_s \quad (40)$$

$$u = u_0, p = p_0, T = T_0 \text{ at } z = 0 \quad (41)$$

$$Y_k = Y_{k0} \text{ (} k = 1, \dots, N_g \text{) at } z = 0 \quad (42)$$

$$0 = \begin{bmatrix} u \\ p \\ T \\ r \end{bmatrix} \Big|_{\psi=\psi_N} - \begin{bmatrix} 0 \\ p_{N-1} \\ T_{\text{wall}} \\ r_{\text{max}} \end{bmatrix} \quad (43)$$

$$\text{State and Control Constraints}(x, q) \quad (44)$$

The vector of state variables is

$$x = [Q_1, Q_2, \dots, Q_N, \theta_1, \dots, \theta_{N_s}],$$

and the control variable is

$$q = T_{\text{wall}}(z).$$

3.2 Direct method

To transform the optimal control problem (37)-(44) to a finite dimensional optimization problem, we apply the direct approach, this means we parameterize the control functions by a finite number of degrees of freedom.

Parameterization of the control functions

The temperature profile at the wall $T_{\text{wall}}(z)$ is treated as control function in the optimal control problem.

Control functions are discretized on an appropriate user-defined grid using a suitable finite functional basis. Usually, the controls are approximated by piecewise continuous functions, e.g., piecewise constant or piecewise linear but also other schemes are applicable. The coefficients in these schemes will be control parameters replacing the control functions. By this way, the control function in infinite-dimensional space is approximated by its piecewise representation using in a finite-dimensional space. If the piecewise linear approximation is applied, then, e.g.,

$$T_{\text{wall}}(z) = T_{\text{wall}}(z_j) + (T_{\text{wall}}(z_{j+1}) - T_{\text{wall}}(z_j)) \frac{z - z_j}{z_{j+1} - z_j}.$$

Note that in this case the bounds on the controls are transformed to bounds on the parameterization coefficients.

Representation of the DAE solution

For given initial values and control parameters, we solve the DAE initial value problem (38)-(43). This yields a representation of the DAE solution which we use for the evaluation of the objective function and the constraints.

3.3 Nonlinear optimization problem

The parameterization of the controls and the states turns the dynamic optimization problem into a finite dimensional optimization problem. It is a nonlinear constrained optimization problem which can be written in abbreviated form as

$$\begin{aligned} \min_v \quad & F(v) \\ \text{subject to} \quad & E(v) = 0 \\ & G(v) \geq 0 \end{aligned} \tag{45}$$

The time-independent control variables q and the control parameters introduced by the parameterization of the control functions are the optimization variables v in the NLP.

3.4 Optimization Methods

To solve constrained nonlinear optimization problems, the method of Sequential Quadratic Programming (SQP) is the most efficient available method. It consists of the solution of a sequence of quadratic optimization problems and can be regarded as a Newton-like method for the optimality conditions of the problem (45). We use the implementation SNOPT [GMS02] which employs BFGS updates for the approximation of the Hessian and an Active-Set strategy for the treatment of the inequalities.

As discussed above, a solution of the semi-discretized PDE only makes sense if the algebraic equations (the boundary condition of the PDE) are consistent. As a consequence, our optimization follows the so-called sequential approach solving the algebraic constraints in every iteration. Fortunately, in our case this is not time consuming and the computing time for consistency calculations is negligible compared to the solution time for the whole discretized PDE.

Computation of derivatives

For the application of the SQP method, derivatives of the objective function and the constraints have to be provided. In our case, this is somewhat intricate because these functions are implicitly defined on the solution of the DAE system derived from the semi-discretization of the PDE.

The derivatives of the DAE solution w.r.t. the control parameters are solution of a variational DAE which, in principle, can be derived by differentiation of the DAE w.r.t. the control parameters. Because discretization of the DAE by a BDF scheme and differentiation commute, we can solve the variational DAE by differentiating the BDF scheme where we freeze all adaptive components as step size and order control and monitor strategy. The step size control is computed from an error estimator for the system consisting of the nominal and variational DAE. Nominal and variational DAE use the same iteration matrix to compute the BDF step. This approach of Internal Numerical Differentiation was introduced by Bock [Boc81] and is implemented in our new BDF code DAESOL.

We apply the automatic differentiation tool ADIFOR (see [BCH⁺95] for more details) to generate Fortran codes for the required derivatives of the model functions of the DAE system. As we described in the previous sections, for our problems, the Jacobian matrices of the model functions are banded-structured. We exploit this structure by seed matrix compression according Curtis, Powell and Reid [CPR74]. This reduces the number of directional derivatives to the total bandwidth of the matrix.

3.5 Optimization Results

For our optimization case study we keep the initial values at the inlet fixed: $X_{\text{C}_2\text{H}_6} = 0.44$, $X_{\text{O}_2} = 0.26$, $X_{\text{N}_2} = 0.30$, the inlet gas temperature $T_{\text{gas}} = 650$ [K], the inlet velocity $u_0 = 0.5$ [m/s].

The wall temperature profile is optimized. We use a piecewise linear parameterization with 8 intervals. Objective is to maximize the mass fraction of ethylene at the outlet. As constraint the temperature is required to be between 600 [K] and 1500 [K].

The optimization was started with a constant temperature profile of 930 [K] leading to an objective value of 0.132. The optimization run took 30 min computational time on a 2.5 GHz Pentium 4 Linux PC. In the optimal solution the objective value is 0.280. Figure 3 shows the temperature profile and figure 4 the mass fraction of ethylene before and after optimization.

The work presented in this paper is the first realization of optimization for this problem.

3.6 Chemical Interpretation of the Results

The results show that temperatures around 1300 K give maximum yield in the ethylene production. At inlet the temperatures only need to be sufficiently high enough for ignition of the combustion to occur. An autothermal reactor – where the temperature is only controlled by the exothermic reaction – should therefore maintain a temperature around 1300 K. This is nearly the same temperature as observed in experiments [HS93]. The optimal oxygen content can be determined by the amount of heat necessary to maintain this temperature.

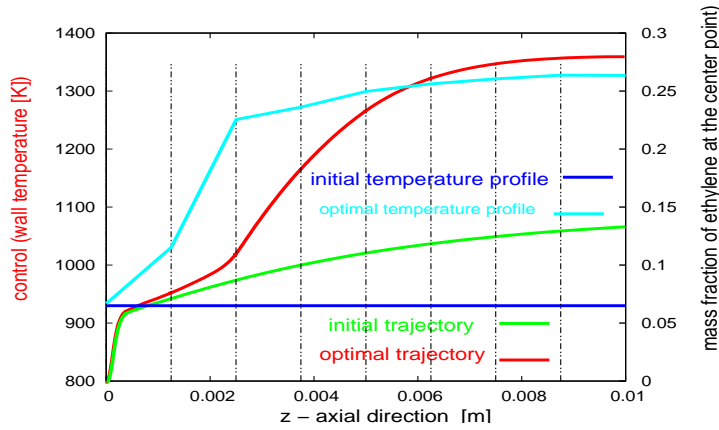


Fig. 3. Initial and optimal temperature profile and initial and optimal trajectory of ethylene at the centerline.

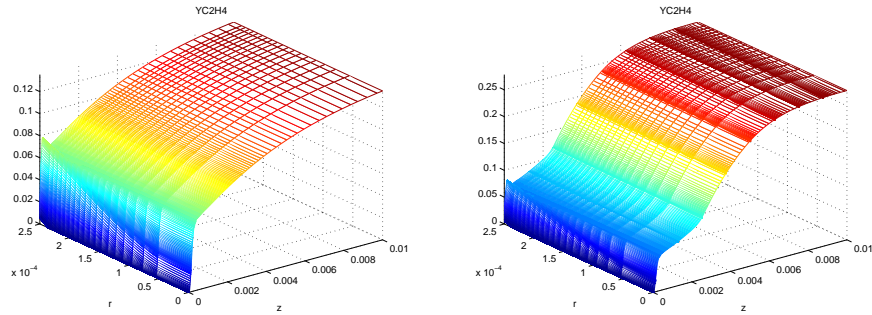


Fig. 4. Initial and optimal profile of ethylene.

4 Conclusions

This project continuous work on conversion of natural gas done previously in the SFB: In [vSDS00] the homogeneous oxidative coupling of methane to achieve ethylene was investigated. By optimization of temperature and residence time the concentration of ethylene could be more than doubled [vSDS00].

In this project, we have developed simulation and optimization software packages for investigating the chemically reacting flow in a catalytic channel. Using the boundary-layer approximation, we model the process by a system of parabolic partial differential equations (PDEs), with nonlinear boundary conditions for coupling gas-phase and surface chemistry. The PDEs are semi-discretized by using the method of lines which leads to a large-scale stiff differential algebraic equations (DAEs). The solution of the DAEs requires a set of consistent initial values. A combination of a time-stepping and of New-

ton's method is employed for finding consistent initial values at the boundary. Based on the BDF code DAESOL, we develop a new code which allows us to solve the DAEs efficiently. Given the inlet conditions and wall temperature profile as parameters, the reactive flow field can be computed very fast, below one minute, even for very complex reaction mechanisms.

The fast simulation of single channel flow fields lets optimization procedures become applicable. Based on the simulation code, we develop the optimization program using the direct approach with an SQP method. The SQP method requires derivatives, which are efficiently computed by the Internal Numerical Differentiation technique.

The program has been applied to the problem of catalyst-supported dehydrogenation of ethane to ethylene. The results are in good agreement with experimental observations. The numerical simulation of the single channel flow field gives detailed insight into the catalytic and gas-phase processes occurring. By this, the program provides a useful tool for the validation of reaction mechanisms.

By the extension to optimization problems the simulation tool has gained a new qualitative level. For the first time, systematic parameter optimization for a reactive tubular flow with detailed chemistry becomes possible. In our case of ethane to ethylene conversion, the temperature profile of the reactor wall was subject to optimization. The ethylene yield could be more than doubled by optimization. The maximum yield was achieved for temperatures around 1300 [K].

Besides the wall temperature, other parameters—such as inlet composition or catalyst distribution along the channel—will be of interest. The method described offers excellent opportunities for further studies of optimization problems.

References

- [BBS99] I. Bauer, H. G. Bock, and J. P. Schlöder. DAESOL – a BDF-code for the numerical solution of differential algebraic equations. Technical report, IWR, University of Heidelberg, 1999. SFB 359.
- [BCH⁺95] Christian Bischof, Alan Carle, Paul Hovland, Peyvand Khademi, and Andrew Mauer. *ADIFOR 2.0 User's Guide*, 1995.
- [BFD⁺97] I. Bauer, F. Finocchi, W. J. Duschl, H.-P. Gail, and J. P. Schlöder. Simulation of chemical reactions and dust destruction in protoplanetary accretion disks. *Astronomy & Astrophys.*, 317:273–289, 1997.
- [Boc81] Hans Georg Bock. Numerical treatment of inverse problems in chemical reaction kinetics. In K. H. Ebert, P. Deuffhard, and W. Jäger, editors, *Modelling of Chemical Reaction System*, volume 18 of *Chemical Physics* 18, pages 102–125. Springer, Heidelberg, 1981.
- [BRF01] A. Beretta, E. Ranzi, and P. Forzatti. Oxidative dehydrogenation of light paraffins in novel short contact time reactors. Experimental and theoretical investigation. *Chemical Engineering Science*, 56(3):779–787, 2001.

- [CKM84] M. E. Coltrin, R. J. Kee, and J. A. Miller. A mathematical model of the coupled fluid mechanics and chemical kinetics in a chemical vapor deposition reactor. *J. Electronchem. Soc.*, 131(2):425–434, 1984.
- [CPR74] A. R. Curtis, M. J. D. Powell, and J. K. Reid. On the estimation of sparse Jacobian matrices. *J. Inst. Math. Appl.*, 13:117–119, 1974.
- [Deu00] O. Deutschmann. *DETCHEM - User manual, version 1.4*. IWR, University of Heidelberg, 2000.
- [GMS02] P. E. Gill, W. Murray, and M. A. Saunders. SNOPT: An SQP algorithm for large-scale constrained optimization. *SIAM J. Opt.*, 12:979–1006, 2002.
- [HS93] M. Huff and L. D. Schmidt. Ethylene formation by oxidative dehydrogenation of ethane over monoliths at very short contact times. *Journal of Physical Chemistry*, 97(45):11815, 1993.
- [Kar97] V. Karbach. *Validierung eines detaillierten Reaktionsmechanismus zur Oxidation von Kohlenwasserstoffen bei hohen Temperaturen*. Diplomarbeit, Universität Heidelberg, 1997.
- [KCG03] R. J. Kee, M. E. Coltrin, and P. Glarborg. *Chemically Reacting Flow: Theory and Practice*. Willey, 2003.
- [RKD⁺00] L. L. Raja, R. J. Kee, O. Deutschmann, J. Warnatz, and L. D. Schmidt. A critical evaluation of Navier-Stokes, boundary-layer, and plug-flow models of the flow and chemistry in a catalytic-combustion monolith. *Catalysis Today*, 59:47–60, 2000.
- [Sch91] W. E. Schiesser. *The Numerical Method of Lines: Integration of Partial Differential Equations*. Academic Press, San Diego, CA, 1991.
- [vSDS00] M. v. Schwerin, O. Deutschmann, and V. Schulz. Process optimization of reactive systems by partial reduced SQP methods. *Computers and Chemical Engineering*, 24:89–97, 2000.
- [WDM96] J. Warnatz, R.W. Dibble, and U. Maas. *Combustion, Physical and Chemical Fundamentals, Modeling and Simulation, Experiments, Pollutant Formation*. Springer-Verlag, New York, 1996.
- [ZAWD00] D. K. Zerkle, M. D. Allendorf, M. Wolf, and O. Deutschman. Understanding homogeneous and heterogeneous contributions to the partial oxidation of ethane in a short contact time reactor. *J. Catal.*, 196:18–39, 2000.

